A microscale analytical study on the strength of two-dimensional frictional granular materials

Alex X. Jerves [a*] & S.A. Galindo-Torres [b]

[a] *College of Science & Engineering, Universidad San Francisco de Quito, Quito Pichincha 1712841 Ecuador*

[b] *School of Engineering, University of Liverpool, L69 3BX UK*

Abstract

We introduce an analytical study of the links between macroscopic strength and the grain-to-grain interactions in two-dimensional frictional granular packings. This study consists of two main parts that are developed and connected progressively. First, we obtain explicit expressions that enable us to relate micro-scale parameters such as contact forces and fabric to macroscopic stress and strength. Second, physical connections and interpretations between the aforementioned micro-parameters, micro-mechanisms, fabric anisotropy and macroscopic strength are derived. Furthermore, throughout this theoretical study, some fundamental physics related to a packing's strength as well as contact buckling is extracted, providing a better understanding of the micro-mechanics that furnishes and builds up the macroscopic strength of this kind of materials.

Keywords: two-dimensional; Mohr-Coulomb; peak friction angle; contact forces; branch vector

*Corresponding author. E-mail: ajerves@usfq.edu.ec (Alex X. Jerves)

1 Introduction

Inhomogeneity and anisotropy are two fundamental properties of granular materials (Rothenburg and Bathurst, 1989) that make them very difficult to model and understand. Hence, granular modeling has been approached from three different perspectives, i.e., experiments, continuum mechanics, and grain-to-grain mechanics, making sometimes difficult to have a well connected framework that includes the three approaches under a unique and comprehensive general theory. Fortunately, nowadays, the increasing computational power, and new experimental techniques, such as, in situ 3D X-ray Computed Tomography (3DXRCT) (Hall et al., 2010), have given rise to new potential bridges that can contribute to connect micro (grain) and macro (continuum) scales by means of experimental, theoretical, and numerical tools that can be applied to the two physical scales (Andrade et al., 2011, 2012).

On the other hand, one of the main challenges in connecting experimental, discrete, and continuum modeling is, precisely, translating micro-scale physical features into their continuum counterparts. Hence, kinetics and topology at the grain scale have, somehow, to be related to continuum typical quantities such as strain and stress, or, in the constitutive sense, to mechanical parameters like internal friction and dilatancy. Thus, a fundamental question rises: what is the micro-mechanical origin of macro-mechanical behavior?, or, in other words: what is the fundamental information that is transmitted from scale to scale?

This work attempts to answer a specify question regarding the micro-macro connections in granular materials, i.e., *how the granular fabric, contacts distribution and boundary conditions affect the failure mode of the particulate assembly?* Thus, for instance, it is well known that a granular packing fails at different values of the deviatoric stress q for different combinations of the principal stresses. This dependence on the *stress path* is a recognized phenomenon which has been described before with anisotropic empirical formulas on the octahedral plane such as the Lade Duncan (Lade and Duncan, 1975) and Matsuoka Nakai (Matsuoka and Nakai, 1982) failure criteria. However, these criteria fail to represent the failure surface of granular packings with highly deformed shapes and contact networks (Galindo-Torres et al., 2013) and provide little insight into the internal physical process since they are fitting forms. To answer our research question, we use concepts such as Mohr-Coulomb's failure criterion (Coulomb, 1776; Chaves, 2009; Borja, 2013), Mohr's circle (Mohr, 1900;

Pytel and Singer, 1987; Oliver and de Saracíbar, 2000), and Coulomb's friction law (Coulomb, 1776; Dowson, 1997), as well as purely mechanical derivations. All these elements will be wrought together to derive general formulae, based on first principles, for two-dimensional assemblies to determine constitutive parameters such as the so-called maximum internal friction angle Φ_{lim} in terms of the stress direction, grains positions and contact network. Figure 1, shows schematically the different components of the theoretical formulation herein proposed to directly connect the macroscopic peak strength of a granular material to its granular counterparts. Furthermore, note that three-dimensional granular packings have not been considered in the present work due to a significant increase in the rotational degrees of freedom of the grains. This adds more difficulty in the mathematical modeling process and the subsequent interpretation of results. Thus, our first goal is to begin by unraveling the grain-to-grain mechanisms behind macroscopic strength in two-dimensional granular materials that, in contrast to their three-dimensional counterparts, lend themselves to a simpler and more minimalistic analysis.

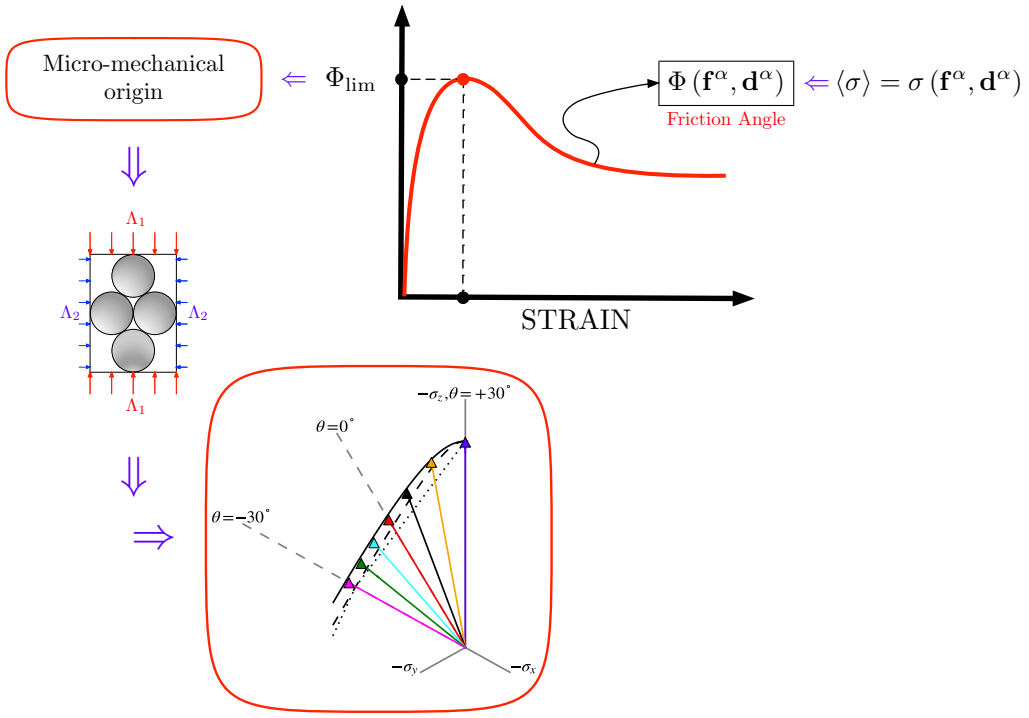

Figure 1: Pictorial sketch of the subjects tackled by the present work and its corresponding contributions. The mathematical relations derived in this study will be based on microscopic features such as the grain positions and the contacts network to obtain the peak internal friction angle $\Phi_{\lim}$. The formalism developed in this study can be extended to 3D to obtain the failure surface for all the possible stress paths which show an inherit anisotropy as seen in micro-mechanics simulations extracted from (Galindo-Torres et al., 2013) and depicted at the bottom of the figure.

Once the described theoretical expressions have been found, we attempt to answer another fundamental question: can these relations be used to draw physical conclusions about the maximum strength $\Phi_{\lim}$ inherent to a given granular packing? Thus, in order to answer this question and to validate the aforementioned theoretical expressions a simple and intuitive example is then used. Hence, some important features about strength, anisotropy, and contact buckling are extracted providing a deeper insight into the mechanical behavior of frictional non-cohesive granular media under confinement.

Finally, a numerical experiment is carried out in order to validate the theoretical framework introduced in the present work. In addition, it is worth mentioning that, even though more complex and tedious, the obtention of a similar type of expressions, relations, analysis, and conclusions for three-dimensional packings of arbitrary shape/size non-cohesive particles can be done by following the same methodology.

2 Peak friction angle

In many important cases, there is no need to know more information about the strength of a given granular material, but only the value of the peak friction angle Φ_{lim} shown in Figure 2. This single parameter usually provides enough information to make decisions in terms of engineering design or prevention. Hence, it is important to have ways and expressions that allow us to compute the value (or a good enough approximation) of the maximum friction angle corresponding to a given granular media.

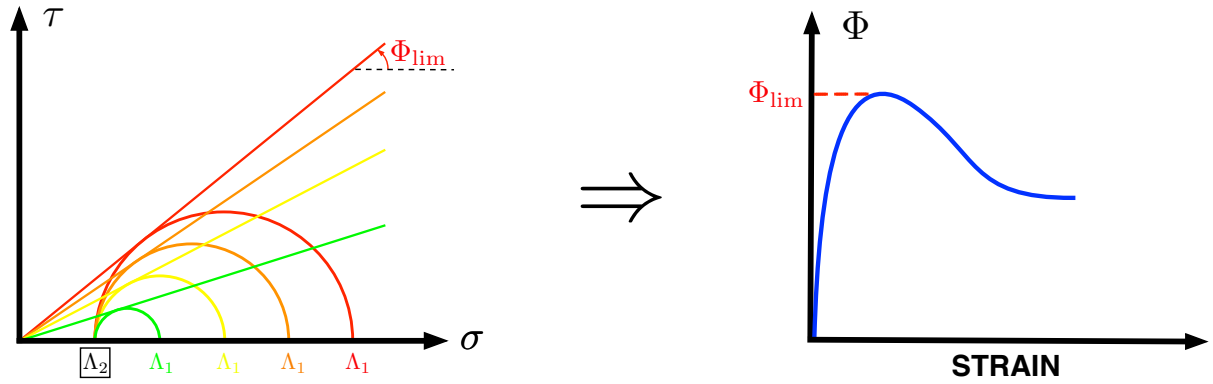

Figure 2: Limit friction angle, Φ_{lim}, defined as the maximum strength reached by a given packing of granular materials as its second principal stress Λ_2 is kept constant while its first principal stress Λ_1 (the most compressive) increases. Here, σ is used in a general way for any volumetric/normal stress.

We now aim to answer a fundamental question that rises at the heart of theoretical granular mechanics: *Does the peak strength, Φ_{lim}, (see Figure 2) inherent to a granular media under confinement depend only on the topology (fabric) of the packing, or this mechanical property is also a function of contact forces and their evolution as a response of the media to a given macro-loading process?* A few theoretical answers (with experimental validation) to such a relevant question have been found for very specific cases, as for instance, regular packings (Rowe, 1962; Horne, 1965; Bishop, 1954) where it is geometrically shown, for this particular type of assemblies, that the maximum strength (and corresponding maximum stress ratio) depends only on the fabric and inter-particle friction coefficient. Hence, in the present work, we look for more general analytical-theoretical ways of unraveling the micro-mechanical origin of the maximum macro-strength of a broader variety of granular assemblies such as those made of polydisperse non-cohesive two-dimensional discs, and

special cases falling into this group.

2.1 Basic assumptions (coordination number)

Every physical theory or mathematical model needs some basic assumptions to define its scope and the ways in which reality is approached. Here, we look at arrays which are packed enough, so its initial topology (at hydrostatic pressure) undergoes a negligible change until the peak (maximum) friction angle Φ_{lim} is reached in a given loading process.

Thus, results from (Kruyt, 2012; Rothenburg and Kruyt, 2004) suggest that, in general, *dense (dilative) granular packings undergo a change of less than* 10% *in their mean coordination number from the initial configuration (hydrostatic confinement) until reaching peak strength.* Here, we define the mean coordination number z as in (Hinrichsen and Wolf, 2004). Finally, we also assume that conditions such as quasi-static loading and small deformations also hold for the present work.

2.2 Mechanical approach

Let us begin the discussion by decomposing the contact force $\boldsymbol{f}^\alpha$, at the α-th contact point between two grains in a packing, into its corresponding components in the normal $\hat{\boldsymbol{r}}^\alpha$ and tangent $\hat{\boldsymbol{t}}^\alpha$ directions as shown by Figure 3.

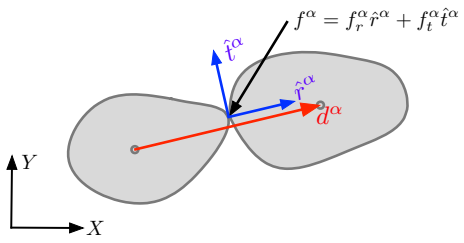

Figure 3: Inter-particle contact force represented in its normal and tangent (to the contact point) components.

Hence, we write $\boldsymbol{f}^\alpha = f_r^\alpha \hat{\boldsymbol{r}}^\alpha + f_t^\alpha \hat{\boldsymbol{t}}^\alpha$, where $\hat{\boldsymbol{r}}^\alpha = \sin(\phi^\alpha)\hat{\boldsymbol{e}}_1 - \cos(\phi^\alpha)\hat{\boldsymbol{e}}_2$, and $\hat{\boldsymbol{t}}^\alpha = \cos(\phi^\alpha)\hat{\boldsymbol{e}}_1 + \sin(\phi^\alpha)\hat{\boldsymbol{e}}_2$, and where, ϕ^α is the angle between the unit vector tangent to the α-th contact point $\hat{\boldsymbol{t}}^\alpha$, and the x-axis (global frame of reference). Here, $\hat{\boldsymbol{e}}_1$ and $\hat{\boldsymbol{e}}_2$ are the basis vectors corresponding to the global (cartesian) frame of reference. In the same way, the branch vector, $\boldsymbol{d}^\alpha$, at the α-th contact point (vector connecting the centroids of two particles in contact at the α-thcontact point)

is expressed in components as $\boldsymbol{d}^\alpha = d_1^\alpha \hat{\boldsymbol{e}}_1 + d_2^\alpha \hat{\boldsymbol{e}}_2 = |\boldsymbol{d}^\alpha| \cos(\delta^\alpha)\, \hat{\boldsymbol{e}}_1 + |\boldsymbol{d}^\alpha| \sin(\delta^\alpha)\, \hat{\boldsymbol{e}}_2$, where δ^α is the angle between $\boldsymbol{d}^\alpha$ and the x-axis (see Figure 3).

Now, from Figure 4, and taking into account that for the case of packings of discs: $\phi^\alpha = \delta^\alpha + \pi/2$, let us write as well the values of the normal and tangent components of a contact force in the following way: $f_r^\alpha = \lambda_1^\alpha \sin(\delta^\alpha) + \lambda_2^\alpha \cos(\delta^\alpha)$ and $f_t^\alpha = \lambda_2^\alpha \cos(\delta^\alpha) - \lambda_1^\alpha \sin(\delta^\alpha)$, where λ_1^α and λ_2^α are the resultant vertical and horizontal forces acting on two particles in contact at the α-th contact point and undergoing quasi-static equilibrium (here we assume compression to be always positive). Furthermore, note that in order to satisfy static equilibrium of torques at the q-th particle, and provided that Coulomb's friction law ($|f_t^\alpha| \leq \mu f_r^\alpha,\ \forall f_r^\alpha \geq 0$) holds, then $M_{\text{act}}^q \leq M_{\text{react}}^q$, where M_{act}^q and M_{react}^q are the total moments acting and reacting on the centroid of the q-th particle, and μ is the inter-particle friction coefficient.

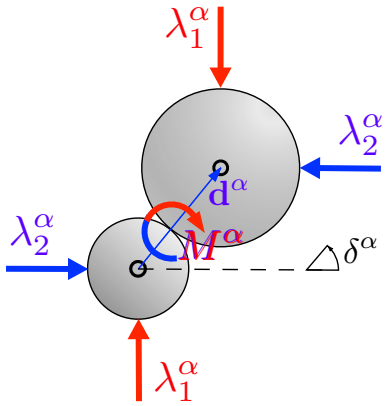

Figure 4: Total resultant forces, λ_1^α and λ_2^α, and moment, M^α, acting on two discs in contact at the α-th contact point.

Thus, combining the expressions for f_r^α and f_t^α with the inequality of static equilibrium of torques, we arrive to the following expression

$$\left.\frac{\lambda_1}{\lambda_2}\right|^\alpha \leq \cot(\alpha^\alpha - \phi_\mu) \tag{1}$$

where, $\alpha^\alpha = \pi/2 - \delta^\alpha$, and $\phi_\mu = \arctan(\mu)$. Moreover, it can be geometrically shown that, for regular packings $\lambda_1 = \Lambda_1 L_1/N_1$ and $\lambda_2 = \Lambda_2 L_2/N_2$, where Λ_i, L_i, and N_i (i = 1,2) are the principal stresses, length of the boundary on which Λ_i is applied, and number of boundary contacts on the boundary of length L_i. Hence, note that using inequality (1), these last expressions, and re-writing

L_i in terms of α, ϕ_μ, and N_i, we arrive to

$$\left.\frac{\Lambda_1}{\Lambda_2}\right|_{\text{lim}} = \cot\left(\alpha - \phi_\mu\right) \frac{2\cos\left(\alpha\right) + 1/N_2}{2\sin\left(\alpha\right) + 1/N_1}$$

as in (Tu and Andrade, 2008). Furthermore, note that as the number of particles in a regular array goes to infinity, N_1 and N_2 also go to infinity and the last expression tends to

$$\left.\frac{\Lambda_1}{\Lambda_2}\right|_{\text{lim}}^{\alpha} = \cot(\alpha - \phi_\mu)\cot(\alpha) \tag{2}$$

which corresponds to Rowe's theory (Rowe, 1962) for mono disperse packings. Thus, bearing this procedure in mind, and as a natural "next step" we now try to obtain a generalization for polydisperse packings as the one illustrated by Figure 5.

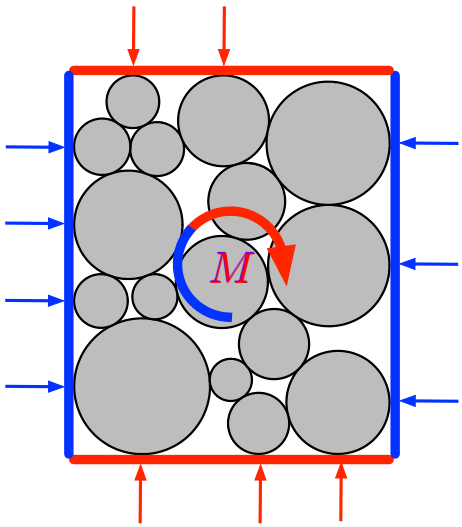

Figure 5: Mismatch in the position/simmetry of the boundary contacts produces a moment M that is distributed "uniformly" along the internal contact points.

Then, for such type of packings, the following expression for λ_i is obtained

$$\lambda_i^\alpha \simeq \underbrace{\frac{\Lambda_i L_i}{Nbc_i}}_{\substack{\text{i-th axial} \\ \text{Load}}} + \underbrace{\frac{M_M}{d_i^\alpha Nc}}_{\substack{\text{Boundary} \\ \text{Mismatch}}} \tag{3}$$

where, Nc is the total number of internal contact points (not boundary contact points included)

in the packing of particles, and Nbc_i is the number of boundary contacts corresponding to one of the boundaries (any of the two boundaries) perpendicular to the direction of Λ_i. Note that the the mismatch moment, M_M, can be split into the sum of two moments, $M_M = M_{M_1} + M_{M_2}$, corresponding to the mismatch moments of the boundaries perpendicular to Λ_1 and Λ_2. Now, expressing the moment at the α-th contact point in terms of M_M, and applying a similar procedure as for the mechanical derivation of expression (2) we obtain the following approximation for the peak ratio $\Lambda_1/\Lambda_2|_{\text{lim}}$ with respect to the α-th contact point (see, Appendix):

$$\left.\frac{\Lambda_1}{\Lambda_2}\right|_{\text{lim}}^{\alpha} \simeq \frac{L_2}{L_1}\frac{Nbc_1}{Nbc_2}\frac{\dfrac{\Delta d_2^{\lambda_1}}{Nc|\mathbf{d}^\alpha|\cos(\delta^\alpha)} - \left[1 + \dfrac{\Delta d_2^{\lambda_2}}{Nc|\mathbf{d}^\alpha|\sin(\delta^\alpha)}\right]\tan(\delta^\alpha + \phi_\mu^\alpha)}{\dfrac{\Delta d_1^{\lambda_2}}{Nc|\mathbf{d}^\alpha|\sin(\delta^\alpha)}\tan(\delta^\alpha + \phi_\mu^\alpha) - \left[1 + \dfrac{\Delta d_1^{\lambda_1}}{Nc|\mathbf{d}^\alpha|\cos(\delta^\alpha)}\right]} \tag{4}$$

where, $\Delta d_1^{\lambda_1}$, $\Delta d_1^{\lambda_2}$, $\Delta d_2^{\lambda_1}$, and $\Delta d_2^{\lambda_2}$ are "measurements" of the average "misalignment" between the contact points of two parallel boundaries of the packing, and $\Delta d_1^{\lambda_2} \simeq \Delta d_2^{\lambda_1}$ (see, Appendix). Once again, note that in the case in which $Nc \to \infty$, then $Nbc_1 \approx Nbc_2$ and equation (4) becomes

$$\left.\frac{\Lambda_1}{\Lambda_2}\right|_{\text{lim}}^{\alpha} \simeq \frac{L_2}{L_1}\tan\left(\delta^\alpha + \phi_\mu^\alpha\right) \tag{5}$$

Now, expressing L_1 and L_2 in terms of the α-th brach vector, we get $L_1 = k_1^\alpha d_1^\alpha = k_1^\alpha\,|\boldsymbol{d}^\alpha|\sin(\alpha^\alpha)$, and $L_2 = k_2^\alpha d_2^\alpha = k_2^\alpha\,|\boldsymbol{d}^\alpha|\cos(\alpha^\alpha)$. Hence, from equation (5), we arrive to

$$\boxed{\left.\frac{\Lambda_1}{\Lambda_2}\right|_{\text{lim}}^{\alpha} \simeq k^\alpha \cot\left(\alpha^\alpha - \phi_\mu^\alpha\right)\cot\left(\alpha^\alpha\right)} \tag{6}$$

where, $k^\alpha = k_2^\alpha/k_1^\alpha$ is a geometric correction parameter, and departing from the Mohr's circle interpretation of the friction angle Φ (see Figure 2), which gives us

$$\sin(\Phi) = \frac{\tau_{\max}}{\bar{p}} = \frac{\Lambda_1 - \Lambda_2}{\Lambda_1 + \Lambda_2} \quad , \quad 0 \leq \sin(\Phi) < 1 \tag{7}$$

expression (6) can be re-written in the following way

$$\boxed{\sin\left(\Phi_{\text{lim}}^\alpha\right) \simeq \frac{(k^\alpha - 1) - (k^\alpha + 1)\left[\cos\left(2\delta^\alpha\right) - \mu^\alpha \sin\left(2\delta^\alpha\right)\right]}{(k^\alpha + 1) - (k^\alpha - 1)\left[\cos\left(2\delta^\alpha\right) - \mu^\alpha \sin\left(2\delta^\alpha\right)\right]}} \tag{8}$$

Finally, comparing equation (6) to Rowe's expression (2), note the local character (at each contact point) of (6), whereas (2) is, in fact, a global result due to the nature of the packings (regular) from which this was derived. In other words, for the case of regular packings, all the contact points that contribute to the global strength will have the same value of local strength, and, therefore, the entire packing will directly "inherit" the same amount of strength for itself.

Remark 1

Expression (8) computes the peak friction angle of a packing in terms of the "failure" of a given contact point. As it is well known, a packing's failure does not depend only on one contact point, but rather it is given by a set of neighboring contacts "failing" at the same time in a similar fashion. We will reconcile these two apparently different ideas (local and global visions) as well as connect them latter on this work.

2.2.1 Sliding v.s. Rolling

From the mechanical analysis being carried out, note that expression (8) yields a $\Phi^{\alpha}_{\text{lim}}$ for the case in which a contact point "fails" (or buckles) by sliding. However, some contact points also may fail due to rolling. Thus, when a contact point between two particles "fails" by rolling, note that the constraint given by Coulomb's friction law, i.e., $|f_t^{\alpha}| \leq \mu^{\alpha} f_r^{\alpha}$, still holds. However, the tangent component of the force, f_t^{α}, is not close enough to its upper limit, so the corresponding contact will "prefer" to "fail" by rolling, meaning that f_t^{α} *is still independent enough on its corresponding normal contact force,* f_r^{α}, and, therefore, the process of rolling is not dependent on the inter-particle friction coefficient μ^{α} (see analytical proof of it on (Jerves and Andrade, 2015)). Thus, μ^{α} can be neglected in expression (8), that becomes

$$\boxed{\sin^{*}\left(\Phi^{\alpha}_{\text{lim}}\right) = \frac{\left(k^{\alpha}-1\right)-\left(k^{\alpha}+1\right)\cos\left(2\delta^{\alpha}\right)}{\left(k^{\alpha}-1\right)-\left(k^{\alpha}+1\right)\cos\left(2\delta^{\alpha}\right)}} \tag{9}$$

On the other hand, and for a general loading process, detecting which particles will fail by rolling and which particles will fail by sliding becomes a whole new issue. However, in the particular case of quasi-static loading this problem becomes a little simpler. Here, we discuss an even simpler version that is valid only for the case of packings of arbitrary size discs.

Inner contacts: In such case, note that the equation of equilibrium of torques for each disc, p, can be expressed in terms of the normal (which vanishes) and tangent components of the contact forces in the following form

$$\sum_{\alpha=1}^{Nc^p} f_t^{\alpha,p} = 0 \tag{10}$$

where, Nc^p is the number of internal contact points corresponding to the disc p. Furthermore, note that an internal disc playing some role in the structural strength of a given packing where it belongs to, necessarily will have to satisfy the constraint $Nc^p \geq 2$. Moreover, under quasi-static loading the sum of torques on each internal disc, p, satisfying $Nc^p \geq 2$, will tend to reach equilibrium as in equation (10), which, in other words, means that the disc will always tend to "fail" by sliding rather than rolling (rotational forces that make the disc roll cancel out), which implies that if a given contact point "fails", it will "fail/yield" by sliding. Hence, when a polydisperse packing of discs "fails", the mechanism governing the micro-mechanical behavior of the packing is sliding (see analytical proof of it on (Jerves and Andrade, 2015)). Moreover, it is worth mentioning that the process just described has to be implemented as part of the algorithm, so the number of structurally relevant contact points that may fail by sliding and rolling can be computed.

Boundary contacts: Now, in order to finish with this discussion, and having analyzed the case of internal discs, let us also analyze what happens for boundary discs. Thus, a boundary disc that only has one internal contact point, $Nc^p = 1$, and shares the rest of its contact points with the walls (which are assumed to be frictionless), will never satisfy equilibrium of torques, expressed for each disc, p, by equation (10), and therefore, its internal contact point will always tend to fail by rolling regardless the value of the inter-particle friction coefficient at that internal contact point. Hence, since this case will not be likely to happen, then most contact points will fail due to sliding.

Thus, and for the case of arbitrary size discs, we use the algorithm described above to detect if a contact point will fail either by sliding or rolling.

2.2.2 Strength Directionality

As part of the physical-geometrical interpretation of the equations that we have derived so far, we also have to look at the directionality of the strength in a given packing of grains. In fact, intuition

tells us that, in general, it is not the same loading a confined packing in one given direction as in other different direction. Hence, in equations (8) and (9), we have marked $\sin\left(\Phi_{\lim}^{\alpha}\right)$ with an asterisk symbol $(*)$ so we identify $\sin^{*}\left(\Phi_{\lim}^{\alpha}\right)$ as a previous (raw) result before taking into account directionality of loading. Thus, we have also derived closed analytical expressions that take into account loading directionality for packings of two-dimensional non-cohesive frictional arbitrary size discs, and where $\Lambda_1 \geq \Lambda_2$, being these the principal stresses in the case of bi-axial loading. Finally, the mentioned expressions are grouped in a simple general form, as shown by expression (11)

$$\Lambda_1 \begin{cases} \| \; x-\text{axis} \Rightarrow \sin^{*}\left(\Phi_{\lim}^{\alpha}\right) = \dfrac{\left(k^{\alpha}-1\right)+\left(k^{\alpha}+1\right)\left[\cos\left(2\delta^{\alpha}\right)+\mu^{\alpha}\sin\left(2\delta^{\alpha}\right)\right]}{\left(k^{\alpha}+1\right)+\left(k^{\alpha}-1\right)\left[\cos\left(2\delta^{\alpha}\right)+\mu^{\alpha}\sin\left(2\delta^{\alpha}\right)\right]} \\ \\ \| \; y-\text{axis} \Rightarrow \sin^{*}\left(\Phi_{\lim}^{\alpha}\right) = \dfrac{\left(k^{\alpha}-1\right)-\left(k^{\alpha}+1\right)\left[\cos\left(2\delta^{\alpha}\right)-\mu^{\alpha}\sin\left(2\delta^{\alpha}\right)\right]}{\left(k^{\alpha}+1\right)-\left(k^{\alpha}-1\right)\left[\cos\left(2\delta^{\alpha}\right)-\mu^{\alpha}\sin\left(2\delta^{\alpha}\right)\right]} \end{cases} \begin{cases} 0 < \sin^{*}\left(\Phi_{\lim}^{\alpha}\right) < 1 \;\rightarrow\; \sin\left(\Phi_{\lim}^{\alpha}\right) = \sin^{*}\left(\Phi_{\lim}^{\alpha}\right) \\ \\ \sin^{*}\left(\Phi_{\lim}^{\alpha}\right) \leq 0 \;\rightarrow\; \sin\left(\Phi_{\lim}^{\alpha}\right) = 0 \\ \\ \sin^{*}\left(\Phi_{\lim}^{\alpha}\right) \geq 1 \;\rightarrow\; \sin\left(\Phi_{\lim}^{\alpha}\right) = 1 \end{cases} \tag{11}$$

Note that expression (11) has two equations: the upper equation holds for the case in which Λ_1 (the first principal stress / most comrpessive) is parallel to the x-axis, and the lower equation holds for the case in which Λ_1 is parallel to the y-axis. Then, the three conditions to the right of the two aforementioned equations have to be applied depending on the values of $\sin^{*}\left(\Phi\right)$ given by them. Finally, a very simple example illustrated by Figure 6 is used to clarify the notions of strength directionality so far analysed.

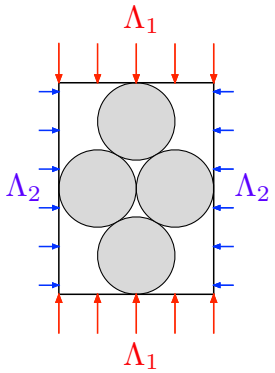

Figure 6: Example of buckling and strength directionality in a regular packing.

This didactic example (see Figure 6) consists of a regular packing of four discs undergoing bi-axial loading. Thus, the components of the force at packing's central contact point at limit (maximum) friction angle, are $f_r^c = 0$ and $f_t^c = 0$. Note that this result is very intuitive in the

physical sense, and can be interpreted as the lost of contact at the central contact point, which makes the entire packing lose stability, making it buckle (fail). As the packing itself can be thought as a column made of a confined granular material (the confinement is provided by Λ_2) carrying a vertical load Λ_1 that reaches its critical (limit or maximum) value at

$$\frac{\Lambda_1}{\Lambda_2}\bigg|_{\text{lim}}^{\alpha} = \cot(\alpha - \phi_\mu)\cot(\alpha)$$

which corresponds to Rowe's theory (Rowe, 1962) that was also substantiated by Horne (Horne, 1965), who assumed no rolling between groups of particles as a constraint. A similar result was previously obtained by Bishop (Bishop, 1954) but expressed in terms of the residual strength. The analysis above holds if Λ_1 is parallel to the y-axis. However, note that if Λ_1 is parallel to the x-axis, then the central contact point yields $\sin(\Phi^c_{\text{lim}}) = 1$, which strengthen the granular packing and gives a point where (in that case) the packing will never fail.

Furthermore, the same intuitive results can be rigorously obtained by a simple analysis of the example given by Figure 6. Thus, using the expression for $\tau_{\max}$ and $\bar{p}$ in terms of branch vectors and contact forces derived in (Jerves and Andrade, 2015) for arbitrary size discs (see, Appendix), we arrive to the following expression for the internal friction angle:

$$\sin(\Phi) = \frac{2f_r - f_r^c}{4f_r + f_r^c}$$

where, f_r^c is the normal component of the central contact point as before, and f_r is the normal component of the contact forces of the rest of internal contact points (which are equal by symmetry). Then, note that as $f_r^c \to 0$, $\sin(\Phi) \to 0.5$, and $\Phi \to 30^o$ corresponding to the case in which Λ_1 is parallel to the y-axis (vertical axis). Moreover, it is worth mentioning that in this particular case, Φ_{lim} does not depend on f_r, and, therefore, it does not depend on f_t either. Hence, Φ_{lim} is not a function of μ as can also be concluded from DEM (Cundall and Strack, 1979) simulations. Furthermore, note that in this particular example, the discs do not roll due to the symmetry of the torques and, therefore, the procedure described in the subsection 2.2.1 does not have to be taken into account.

On the other hand, when $f_r^c \to \infty$, $|\sin(\Phi)| \to 1$, and $\Phi \to 90^o$, which implies infinite strength,

and corresponds to the case in which Λ_1 is parallel to the x-axis (horizontal axis). Note as well that the case in which $f_r \to \infty$ is equivalent to the case $f_r^c \to 0$, so yields the same result and corresponding interpretation. Moreover, the case $f_r \to 0$ implies that no external loading nor confinement are being applied and yields a peak friction angle $\Phi = 90^o$ that means infinite strength, which is expected as well.

Finally, in order to wrap up this section, lets compare these results with a general "big enough" polydisperse packing, where there is very little to none symmetry as opposed to the example above. Then, for the polydisperse packing, most contacts will "fail" by sliding, as already concluded in subsection 2.2.1. However, sets of neighboring discs with some symmetrical features will tend to form clusters that, in turn, display the rolling-like type of mechanisms (crystalline type of structure) found in this example. Thus, mesoscale-like clusters will appear whenever symmetrical features are found, playing a key role in the overall packing's strength and its variability as the main loading direction changes.

2.3 Global Solution

As mentioned in Remark 1, expression (8) computes the peak friction angle of a packing in terms of the "failure" of a given contact point, which does not actually corresponds to the "whole" packing's failure that is actually given by a set of neighboring contacts "failing" at the same time in a similar fashion. Hence, we need to detect the aforementioned set by computing the value of $\Phi_{\text{lim}}^{\alpha}$ for every single inner contact point in the packing and then "assess" which are the ones that are actually in their maximum local strength values as well as clustering at the same time. As this assessment can get as sophisticated as wanted, we have found a simple and accurate enough way of approaching it. Thus, a packing's (global) maximum strength Φ_{lim} can be approximated in terms of the mean value theorem for integrals, which, and for simplicity in the computational implementation, we combine with the trapezoid rule for numerical integration, arriving to the following expression:

$$\boxed{\left\langle \sin\left(\Phi_{\text{lim}}\right)\right\rangle = \frac{1}{2\left(\delta_{\max} - \delta_{\min}\right)} \sum_{\alpha=1}^{Nc-1} \left[\sin\left(\Phi_{\text{lim}}^{\alpha}\right) + \sin\left(\Phi_{\text{lim}}^{\alpha+1}\right)\right]\left(\delta^{\alpha+1} - \delta^{\alpha}\right)} \tag{12}$$

Note that any other numerical scheme can also be used. However, we have chosen the trapezoid rule since the nature of the problem does not require applying a more accurate numerical scheme

due to the shape of the distribution of the values of $\Phi^{\alpha}_{\text{lim}}$ in terms of de branch vector's angles δ^{α} as shown by Figure 7 for the packing shown in Figure 8, and for an inter-particle friction coefficient $\mu = 0.5$. Furthermore, note from Figure 7 that the distribution of values corresponding to $\langle \sin(\Phi_{\text{lim}}) \rangle$ will be non-linearly scaled from the one given for $\Phi^{\alpha}_{\text{lim}}$, to values between 0 and 1 in the y-axis, since one can be directly computed from the other. Thus, in either case the trapezoid rule can be applied with the similar accuracy. Note as well that as the number of contact points with different directions increases, the accuracy of the value obtained for $\langle \sin(\Phi_{\text{lim}}) \rangle$ by applying the trapezoid rule (or any other method to perform the corresponding numerical integration) will increase.

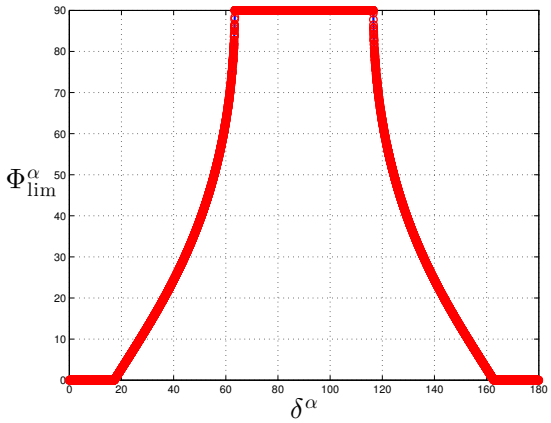

Figure 7: Distribution of the local maximum friction angles $\Phi^{\alpha}_{\text{lim}}$ v.s. their corresponding branch vector's angles δ^{α} for the granular packing given by Figure 8 and for an inter-particle friction coefficient $\mu = 0.5$.

Thus, the packing's (global) maximum strength Φ_{lim} has been found here to be nothing but the "mean" (understood under the umbrella of the mean value theorem for integrals) of all the maximum (peak) values of the friction angle $\Phi^{\alpha}_{\text{lim}}$ given for each α-th structurally relevant contact point (local solution) as shown by Figure 7 for an inter-particle friction coefficient of $\mu = 0.5$. In other words, the packing's maximum strength Φ_{lim} is the "mean" of all the structurally relevant local frictional strengths $\Phi^{\alpha}_{\text{lim}}$.

2.4 Implementation

It is worth mentioning that when it comes to the computational implementation of the theoretical framework herein introduced, every step described has to be taken into account, i.e., mechanical and geometrical interpretations, sliding v.s. rolling, and strength directionality as described in the previous sections of the present work.

3 Example

In this example we have a two-dimensional polydisperse packing (see Figure 8) composed of 5752 discs with average diameter of 0.6 units, and standard deviation of 0.23 units. The walls of the packing have a friction coefficient of $\mu_w = 1E^{-6}$. The packing departs from a hydrostatic state of stress corresponding to 100 units of pressure, and then, undergoes quasi-static axial loading along the vertical axis while keeping the horizontal stress constant. This numerical experiment is carried out by using the contact dynamics model introduced in (Krabbenhoft et al., 2012a,b), where: $k_r = k_t = 7.5E^4$ (units of force per unit of length) are the effective normal and tangent stiffness, $\dot{u}_2 = 7.5E^{-6}$ (units of length per unit of time) is the vertical loading velocity at the upper wall, and $\theta = 1$ (backward Euler, i.e., implicit integration) is a numerical integration parameter, which yields a coefficient of restitution of zero (perfectly inelastic collision).

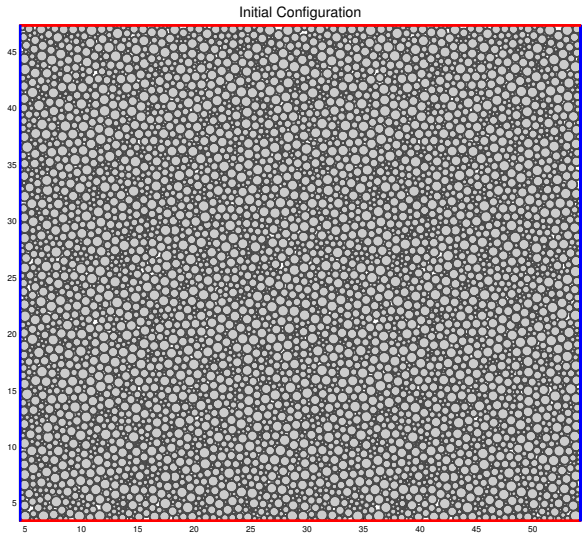

Figure 8: Polydisperse packing of 5752 discs. The discs are confined by a rectangular container ($\sim 49.8 \times 44$ square units) with quasi-frictionless walls ($\mu_w = 1E^{-6}$). The packing is subjected to quasi-static axial loading along the vertical axis and departs from a state of hydrostatic loading of 100 units of pressure.

Then, after running a new simulation for each different value of the inter-particle friction coefficient ($\mu = 0.01,\ 0.05,\ 0.1,\ 0.2,\ 0.3,\ 0.4,\ 0.5,\ 0.6,\ 0.7,\ 0.8,\ 0.9,\ 1$) while keeping all the other parameters and conditions the same, the maximum strength Φ_{lim} for each μ was obtained. Figure 9 shows a comparison between the actual peak friction angle (blue line) of the packing shown by Figure 8 (computed directly from the numerical DEM-simulation), and the theoretically predicted peak friction angle (red line) for different values of the inter-particle friction coefficient μ (Procter and Barton, 1974). As can be noticed from Figure 9, the two curves are very similar with an average error of 6.14% and an average mismatch of 1.1°. The same type of simulation has been carried out for similar packings with 2876 and 1438 particles, giving an average error of 6.49% and 5.80%.

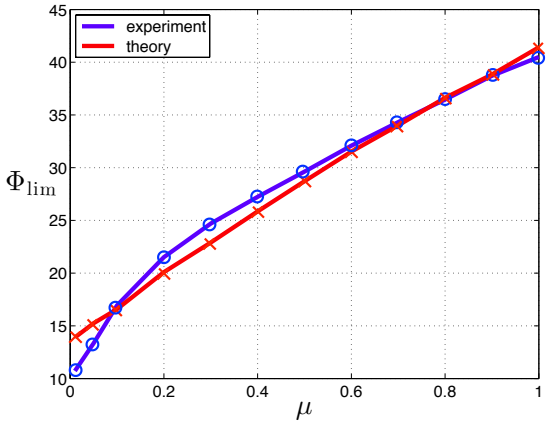

Figure 9: Peak friction angle Φ_{lim}, corresponding to the granular packing introduced by Figure 8, and in terms of the inter-particle friction coefficient μ (0.01, 0.05, 0.1, 0.2, 0.3, 0.4, 0.5, 0.6, 0.7, 0.8, 0.9, 1): numerical experimentation (blue line), and analytical approach (red line).

Finally, note that for high enough values of μ ($\mu \geq 0.5$) the error in the theoretical approximation becomes negligible. On the other hand, note that there is some error for values of $\mu < 0.5$. This error increases as $\mu \to 0$, and it is due to the fact that, from a thermodynamical point of view (Borja, 2013), a purely frictionless material is not feasible. This is translated into the numerical model (DEM) results as a non-physical behavior for small enough values of μ (Jerves and Andrade, 2015), that can be clearly seen in Figure 9 by taking a look at the drastic change of slope given for $\mu \leq 0.2$ in the results corresponding to the numerical experimentation (blue line). Moreover, some error also comes from the numerical integration scheme (backward Euler) used for the DEM simulation that yields a coefficient of restitution for the discs equal to zero, which, in the same way, is non-physical due to the numerical dissipation added by it.

4 Conclusions and Remarks

We have developed an analytical-theoretical framework that helps us to further understand the physics behind the microscopic origin of macroscopic strength of two-dimensional frictional granular materials. This framework rests on two fundamental theoretical models right at the heart of granular mechanics, i.e., Mohr-Coulomb's failure criterion for the macroscopic behavior, and Coulomb's friction law for the grain-to-grain frictional interactions. Hence, all the findings and

analysis introduced in this work are valid only for the cases where the combination of these two theoretical frameworks applies.

Thus, we have been able to establish explicit connections between micro-mechanical parameters such as contact forces and branch vectors, which in essence describe fabric and contact kinetics, and macro-mechanical quantities such as stress and the material's strength. In the case of the maximum strength of a packed enough (dilative) packing of non-cohesive polydisperse discs undergoing bi-axial loading, the results suggest that it does not depend on the inter-particle contact forces and their evolution, but on the packings's initial shape, initial fabric, external loading directionality, and on the inter-particle friction coefficient. The dependency on some of these micro-parameters such as initial fabric and inter-particle friction coefficient has already been discussed by (Rowe, 1962), but for the more specific case of monodisperse regular packings. Furthermore, one of our main findings is that *for a given polydisperse packing, its (global) maximum strength* Φ_{lim} *can be computed as the mean (in terms of the mean value theorem for integrals) of the local "maximum strenghts" of all "failing" contact points within such packing.* Further analysis on rolling and sliding mechanisms of contact "failure" as well as strength directionality (anisotropy) have to be taken into consideration in order to arrive to the aforementioned result and shed more light on the discussion.

Finally, it is worth mentioning that the theoretical framework developed throughout the present work can also be extended to three-dimensional packings of non-cohesive frictional arbitrary shape/size grains. This can be done by parametrizing the stress path in the three dimensional principal stresses space before applying an optimization process such as Karush-Kuhn-Tucker (KKT) conditions (Karush, 1939; Kuhn and Tucker, 1951; Kuhn, 2007). This will provide failure surfaces based on first principles, which will replace the empirical surfaces that are commonly used to describe the strength of soils under triaxial conditions. We attempt to plant a first seed that may help to start the conversation on the potential applications and generalizations of the introduced analytical framework, not only for three-dimensional packings, but also to help us acquire a deeper understanding of related physical phenomena such us force chains and shear banding. In the future, the process that was described herein can become practical if statistical information on the branch vector and force distributions is included into the Moore-Love expression (Bagi, 1999; Saxce et al., 2004; Love, 1927; Weber, 1966; Rothenburg and Selvadurai, 1981; Christoffersen et al., 1981; Oda

and Iwashita, 1999) for the average Cauchy stress of a packing of grains as follows,

$$\sum_{\alpha=1}^{Nc} \boldsymbol{d}^{\alpha} \otimes \boldsymbol{f}^{\alpha} = \sum_{d,f} p\left(\boldsymbol{d}, \boldsymbol{f}\right) \otimes \boldsymbol{f}$$

where the new summation is done over all the possible values of $\boldsymbol{d}$ and $\boldsymbol{f}$ instead of each contact, and $p\left(\boldsymbol{d}, \boldsymbol{f}\right)$ is the probability that a given contact has a branch vector with value $\boldsymbol{d}$ and contact force with value $\boldsymbol{f}$. Accurate approximations for such statistics already exist in the literature (Radjai et al., 1996) and the combination of these features into the proposed framework should be the subject of future research.

Appendix

Peak friction angle

Note that λ_1^{α} can be decomposed as follows:

$$\lambda_i^{\alpha} = \lambda_{i\,\Lambda_i}^{\alpha} + \lambda_{i\,x}^{\alpha} + \lambda_{i\,y}^{\alpha}$$

where $i = 1, 2$, and

$$\lambda_{i\,\Lambda_i}^{\alpha} = \frac{\Lambda_i L_i}{Nbc_i} \quad , \quad \lambda_{i\,x}^{\alpha} = \frac{M_{M_i}}{d_i^{\alpha} Nc} \quad , \quad \lambda_{i\,y}^{\alpha} = \frac{M_{M_j}}{d_i^{\alpha} Nc}$$

are the values of λ_i due to the applied boundary stress Λ_i, to the misalignment of the boundaries parallel to the x-axis, and to the misalignment of the boundaries parallel to the y-axis, respectively. On the other hand, by applying equivalent couples, M_{M_i} and M_{M_j} can be re-written as:

$$M_{M_i} \simeq \frac{\Lambda_i L_i}{Nbc_i} \Delta d_i^{\lambda_i} \quad , \quad M_{M_j} \simeq \frac{\Lambda_j L_j}{Nbc_j} \Delta d_j^{\lambda_i}$$

where, $\Delta d_1^{\lambda_1}$, $\Delta d_1^{\lambda_2}$, $\Delta d_2^{\lambda_1}$, and $\Delta d_2^{\lambda_2}$ are "measurements" of the average "misalignment" between the contact points of two parallel boundaries of the packing, and $\Delta d_1^{\lambda_2} \simeq \Delta d_2^{\lambda_1}$. Hence, we have

$$\lambda_1^{\alpha} \simeq \frac{\Lambda_1 L_1}{Nbc_1} + \frac{\Lambda_1 L_1}{Nbc_1} \frac{\Delta d_1^{\lambda_1}}{Nc\,|\boldsymbol{d}^{\alpha}| \cos\left(\delta^{\alpha}\right)} + \frac{\Lambda_2 L_2}{Nbc_2} \frac{\Delta d_2^{\lambda_1}}{Nc\,|\boldsymbol{d}^{\alpha}| \cos\left(\delta^{\alpha}\right)}$$

and,

$$\lambda_2^\alpha \simeq \frac{\Lambda_2 L_2}{Nbc_2} + \frac{\Lambda_2 L_2}{Nbc_2}\frac{\Delta d_2^{\lambda_2}}{Nc\,|\boldsymbol{d}^\alpha|\sin(\delta^\alpha)} + \frac{\Lambda_1 L_1}{Nbc_1}\frac{\Delta d_1^{\lambda_2}}{Nc\,|\boldsymbol{d}^\alpha|\sin(\delta^\alpha)}$$

Now, solving these equations for Λ_1/Λ_2, replacing inequality (1), and assuming that the α-th contact point in this inequality is at "failure", we arrive to equation (4).

Four discs regular monodisperse packing example

From (Jerves and Andrade, 2015), we have

$$\bar{p} = \frac{1}{2V}\sum_{\alpha=1}^{Nc}|\boldsymbol{d}^\alpha|[f_r^\alpha \sin(\phi^\alpha - \delta^\alpha) + f_t^\alpha \cos(\phi^\alpha - \delta^\alpha)]$$

$$\tau_{\max} = \frac{1}{2V}\sqrt{\left\{\sum_{\alpha=1}^{Nc}|\boldsymbol{d}^\alpha|[f_r^\alpha \sin(\phi^\alpha + \delta^\alpha) + f_t^\alpha \cos(\phi^\alpha + \delta^\alpha)]\right\}^2 + \left\{\sum_{\alpha=1}^{Nc}|\boldsymbol{d}^\alpha|\,[f_r^\alpha \cos(\phi^\alpha + \delta^\alpha) - f_t^\alpha \sin(\phi^\alpha + \delta^\alpha)]\right\}^2}$$

where, from Figure 3 we have that

$$\hat{\boldsymbol{r}}^\alpha = \sin(\phi^\alpha)\hat{\boldsymbol{e}}_1 - \cos(\phi^\alpha)\hat{\boldsymbol{e}}_2 \quad , \quad \hat{\boldsymbol{t}}^\alpha = \cos(\phi^\alpha)\hat{\boldsymbol{e}}_1 + \sin(\phi^\alpha)\hat{\boldsymbol{e}}_2$$

with, ϕ^α being the angle between the unit vector tangent to the α-th contact point, $\hat{\boldsymbol{t}}^\alpha$, and the x-axis (global frame of reference); and $\hat{\boldsymbol{e}}_1$, $\hat{\boldsymbol{e}}_2$ being the basis corresponding to the global (cartesian) frame of reference as shown in Figure 3.

Moreover, from the Mohr circles of Figure 2, note that for cohesionless materials

$$\sin(\Phi) = \frac{\tau_{\max}}{\bar{p}} = \frac{\Lambda_1 - \Lambda_2}{\Lambda_1 + \Lambda_2}$$

and, for the case in which the particles are discs, note that $\phi^\alpha = \delta^\alpha + 90^o$. Thus, for polydisperse packings of cohesionless frictional discs undergoing axial loading, we arrive to

$$\sin(\Phi) = -\frac{\displaystyle\sum_{\alpha=1}^{Nc}|\boldsymbol{d}^\alpha|[f_r^\alpha \cos(2\delta^\alpha) - f_t^\alpha \sin(2\delta^\alpha)]}{\displaystyle\sum_{\alpha=1}^{Nc}|\boldsymbol{d}^\alpha| f_r^\alpha}$$

which, for the four discs packing of the example in subsection 2.2.2 where δ^{α} takes the values of 60^o, 120^o, 240^o, 300^o, and 0^o, it becomes

$$\sin(\Phi) = \frac{2f_r - f_r^c}{4f_r + f_r^c}$$

where, f_r^c and f_t^c are the normal and tangent components of the central contact point as before, and f_r, f_t are the normal and tangent components of the contact forces of the rest of internal contact points (which are equal by simmetry, f_t is also the same in absolute value).

References

Andrade, J. E., Avila, C. F., Lenoir, N., Hall, S. A., and Viggiani, G. 2011. "Multiscale modeling and characterization of granular matter: from grain scale kinematics to continuum mechanics". *Journal of the Mechanics and Physics of Solids 59*, 237–250.

Andrade, J. E., Vlahinić, I., Lim, K.-W., and Jerves, A. X. 2012. "Multiscale 'tomography-to-simulation' framework for granular matter: the road ahead". *Géotechnique Letters 2*, 135–139.

Bagi, K. 1999. "Microstructural stress tensor of granular assemblies with volume forces". *Journal of Applied Mechanics 66*(4), 934 – 936.

Bishop, A. W. 1954. "Correspondence on shear characteristics of a saturated silt measured in triaxial compression". *Géotechnique 4*(1), 43–45.

Borja, R. I. 2013. *"Plasticity Modeling and Computation"*. Springer.

Chaves, E. W. V. 2009. *"Mecánica del Medio Continuo: Modelos Constitutivos"*. Barcelona, Spain: International Center for Numerical Methods in Engineering.

Christoffersen, J., Mehrabadi, M. M., and Nemat-Nasser, S. 1981. "A micromechanical description of granular material behavior". *Journal of Applied Mechanics 48*, 339–344.

Coulomb, C. A. 1776. "Essai sur une application des règles de maximus et minimis à quelques problèmes de statique relatifs à l'architecture". *Memoires de Mathématique et de Physique, Présentés a l'Académie Royale des Sciences, par divers Savans, et lûs dans ses Assemblées 7*, 343–382.

Cundall, P. A. and Strack, O. D. L. 1979. A discrete numerical model for granular assemblies. *Géotechnique 29*, 47–65.

Dowson, D. 1997. *"History of Tribology"* (2 ed.). Professional Engineering Publishing.

Galindo-Torres, S. A., Pedroso, D. M., Williams, D. J., and Mühlhaus, H. B. 2013. "Strength of non-spherical particles with anisotropic geometries under triaxial and shearing loading configurations". *Granular Matter 15*(5), 531–542.

Hall, S. A., Bornert, M., Desrues, J., Pannier, Y., Lenoir, N., Viggiani, G., and Bésuelle, P. 2010. "Discrete and continuum analysis of localized deformation in sand using X-ray micro CT and volumetric digital image correlation". *Géotechnique 60*, 315–322.

Hinrichsen, H. and Wolf, D. E. (Eds.) 2004. *"The Physics of Granular Media"*. Weinheim: Wiley-VHC Verlag GmbH & Co. KGaA.

Horne, M. R. 1965. "The behavior of an assembly of rotund, rigid, cohesionless particles parts 1 and 2". *Proceedings of The Royal Society A: Mathematical, Physical and Engineering Sciences 286*(1404), 62–97.

Jerves, A. X. and Andrade, J. E. 2015. "A micro-mechanical study of peak strength and critical state". *International Journal for Numerical and Analytical Methods in Geomechanics 40*, 1184–1202.

Karush, W. 1939. *"Minima of Functions of Several Variables with Inequalities as Side Constraints"*. Msc dissertation, University of Chicago.

Krabbenhoft, K., Lyamin, A., Huang, J., and da Silva, M. V. 2012a. "Granular contact dynamics using mathematical programming methods". *Computers and Geotechnics 241-244*, 262–274.

Krabbenhoft, K., Lyamin, A., Huang, J., and da Silva, M. V. 2012b. "Granular contact dynamics with particle elasticity". *Granular Matter 14*, 607–619.

Kruyt, N. P. 2012. "Micromechanical study of fabric evolution in quasi-static deformation of granular materials". *Mechanics of Materials 44*, 120–129.

Kuhn, H. W. and Tucker, A. W. 1951. "Nonlinear programming". In *Nonlinear programming*, pp. 481–492. Proceedings of 2nd Berkeley Symposium: Berkeley: University of California Press.

Kuhn, M. 2007. "The karush-kuhn-tucker theorem". Cdse seminar, University of Mannheim.

Lade, P. V. and Duncan, J. M. 1975. "Elastoplastic stress-strain theory for cohesionless soil". *Journal of the Geotechnical Engineering Division, ASCE 101*, 1037–1053.

Love, A. 1927. *"A Treatise of Mathematical Theory of Elasticity"*. Cambridge University Press.

Matsuoka, H. and Nakai, T. 1982. "A new failure criterion for soils in three-dimensional stresses". In *Conference on Deformation and Failure of Granular Materials*, pp. 253–263. IUTAM.

Mohr, O. 1900. "Welche umstände bedingen die elastizitätsgrenze und den bruch eines materiales?". *Zeitschrift des Vereines Deutscher Ingenieure 44*, 1524–1530; 1572–1577.

Oda, M. and Iwashita, K. 1999. *"Mechanics of granular materials: an introduction"*. Rotterdam, Netherlands: CRC Press / Balkema.

Oliver, X. and de Saracíbar, C. A. 2000. *"Mecánica de medios continuos para ingenieros"*. Barcelona, Spain: Ediciones UPC.

Procter, D. C. and Barton, R. R. 1974. "Measurements of the angle of interparticle friction". *Géotechnique 24*, 581–604.

Pytel, A. and Singer, F. L. 1987. *"Strength of materials"* (4 ed.). Harper & Row.

Radjai, F., Jean, M., Moreau, J. J., and Roux, S. 1996. "Force distributions in dense two-dimensional granular systems". *Phys. Rev. Lett. 77*, 274–277.

Rothenburg, L. and Bathurst, R. J. 1989. "Analytical study of induced anisotropy in idealized granular materials". *Géotechnique 39*, 601–614.

Rothenburg, L. and Kruyt, N. P. 2004. "Critical state and evolution of coordination number in simulated granular materials". *International Journal of Solids and Structures 41*(21), 5763–5774.

Rothenburg, L. and Selvadurai, A. 1981. "A micromechanical definition of the cauchy stress tensor for particular media". In A. P. S. Selvadurai (Ed.), *Mechanics of Structured Media*, Amsterdam, pp. 469–486. Elsevier.

Rowe, P. W. 1962. "The stress-dilatancy relation for static equilibrium of an assembly of particles in contact". *Proceedings of The Royal Society A: Mathematical, Physical and Engineering Sciences 269*(1339), 500–527.

Saxce, G. D., Fortin, J., and Millet, O. 2004. "About the numerical simulation of the dynamics of granular media and the definition of the mean stress tensor". *Mechanics of Materials 36*(12), 1175–1184.

Tu, X. and Andrade, J. E. 2008. "Criteria for static equilibrium in particulate mechanics computations". *International Journal for Numerical Methods in Engineering 75*, 1581–1606.

Weber, J. 1966. "Recherches concernant les contraintes intergranulaires dans les milieux pulvérulents". *Bulletin de Liaison des Ponts-et-Chaussees 1*(20), 1 – 20.